Structures of the Sea-Breeze Front in Dual-Doppler Lidar Observation and Coupled Mesoscale-to-LES Modeling

doi: 10.1029/2018JD029017

JGR Atmospheres

RESEARCH ARTICLE
10.1029/2018JD029017

Structures of the Sea-Breeze Front in Dual-Doppler Lidar Observation and Coupled Mesoscale-to-LES Modeling

Guixing Chen[1,2], Hironori Iwai[3], Shoken Ishii[3], Kazuo Saito[4,5], Hiromu Seko[4,5], Weiming Sha[6], and Toshiki Iwasaki[6]

[1]School of Atmospheric Sciences, and Guangdong Province Key Laboratory for Climate Change and Natural Disaster Studies, Sun Yat-sen University, Guangzhou, China, [2]Southern Laboratory of Ocean Science and Engineering, Zhuhai, China, [3]National Institute of Information and Communications Technology, Tokyo, Japan, [4]Meteorological Research Institute, Tsukuba, Japan, [5]Japan Agency for Marine-Earth Science and Technology, Yokohama, Japan, [6]Department of Geophysics, Graduate School of Science, Tohoku University, Sendai, Japan

Abstract Sea-breeze front (SBF) can cause dramatic changes in weather and air quality near the coast. However, the observation and forecast of its three-dimensional (3-D) fine-scale structures have been challenging. Using mesoscale-to-large eddy simulations (LES) models and high-resolution lidar measurement over Sendai Airport, here we perform a successful simulation of the observed 3-D structures of an SBF for the first time. We show that frontal structures are characterized by a series of lobes (spaced ~500 m apart) aligned along the raised sea-breeze head, where the shear between sea breeze and alongshore ambient flow aloft is evident. Local strong updrafts occur both in the frontal lobes of marine cold air and in the prefrontal warm air ascending the wedge of windward lobes. Downdrafts form behind the lifted marine cold air and trap air pollutants. These fine-scale structures and vertical motions are repeatedly strengthened by the short-term disturbances of gravity currents that move onshore and collide with the SBF. They are also affected by buildings and determine the detailed variations of surface winds. We conclude that advanced observation and modeling systems can potentially improve the prediction of coastal weather and environment.

Plain Language Summary When sea breeze comes, it does not come gently and often brings a sudden change in winds, temperature, and air quality. The so-called sea-breeze front has great influence on the environment in coastal areas around the world. This work presents a major progress to reveal its fine-scale 3-D structures using the state-of-art observations and numerical models. The dynamics and evolution of the frontal structures are further linked to the disturbances of gravity current and the effect of buildings near the coast. Some differences to the known concept of idealized sea-breeze front are also identified. We believe that the findings have significant impacts on the research community of weather forecast, numerical modeling, and coastal environment studies.

Key Points:
- Lidar observations capture well the fine-scale 3-D structures and evolution of a typical sea-breeze front
- A novel local prediction system can reproduce frontal lobes/clefts and updrafts at high accuracy and resolution
- Gravity current disturbances control the short-term variations of frontal structures, while coastal buildings affect detailed features

Correspondence to:
G. Chen,
chenguixing@mail.sysu.edu.cn

Citation:
Chen, G., Iwai, H., Ishii, S., Saito, K., Seko, H., Sha, W., & Iwasaki, T. (2019). Structures of the sea-breeze front in dual-Doppler lidar observation and coupled mesoscale-to-LES modeling. *Journal of Geophysical Research: Atmospheres*, *124*, 2397–2413. https://doi.org/10.1029/2018JD029017

Received 16 MAY 2018
Accepted 29 JAN 2019
Accepted article online 6 FEB 2019
Published online 2 MAR 2019

Author Contributions:
Conceptualization: Guixing Chen
Funding acquisition: Guixing Chen, Kazuo Saito, Hiromu Seko, Toshiki Iwasaki
Methodology: Guixing Chen, Hironori Iwai, Hiromu Seko, Weiming Sha
Validation: Guixing Chen, Hironori Iwai, Shoken Ishii
Visualization: Guixing Chen, Hironori Iwai
Writing - original draft: Guixing Chen

1. Introduction

Sea breeze occurs in coastal areas around the world, with great impacts on local weather and atmospheric environment. Its onset is usually characterized by the passage of a sea-breeze front (SBF), which resembles a shallow cold front (e.g., Simpson, 1994, 1997). The associated sudden changes in local winds and temperature may affect human activities along coasts, such as sailing, fishing, gliding, aviation, and wind energy industry (e.g., Adams, 1997 ; Miller et al., 2003). The cool marine air behind an SBF also provides relief from hot weather and regulates the urban effect of coastal cities (Hu & Xue, 2016; Inoue & Kimura, 2004). Rising air currents at SBF sometimes lead to cloud formation, trigger convective weather, and disperse airborne insects/pollutants, which are of special interest to weather forecasters and environmental scientists (Atkins et al., 1995; Boyouk et al., 2011; Fovel, 2005; Moncrieff & Liu, 1999; Saito et al., 2018). The structure, dynamics, and impacts of the SBF have been the focus of numerous observational, numerical, and theoretical studies in recent decades (Crosman & Horel, 2010; Miller et al., 2003). Advancing our knowledge of and ability to forecast the SBF has significant societal implications since a large part of the global population lives in coastal regions.

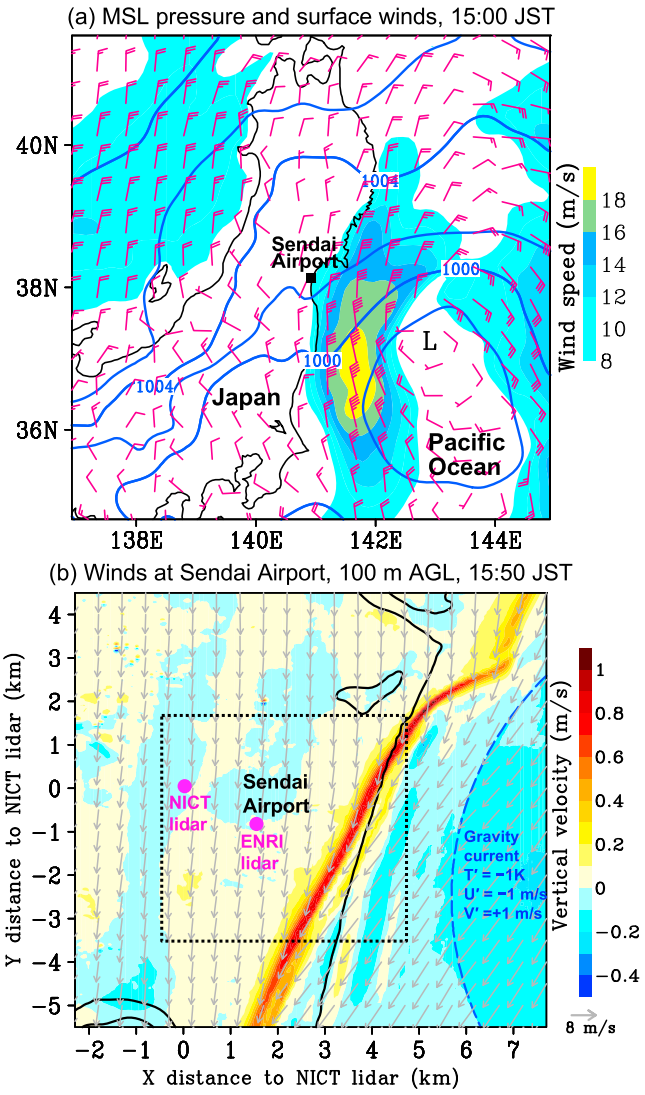

Figure 1. Weather pattern of a backdoor-type sea breeze event. (a) Mean sea level pressure (contour) and surface winds (barbs, shaded for wind speed ≥8 m/s) derived from mesoscale analysis at 15:00 JST on 15 June 2007. (b) Horizontal winds (vector) and vertical motion (shaded) over Sendai Airport derived from the Japan Meteorological Agency-Nonhydrostatic Model forecast at 15:50 JST and used as the initial condition of large eddy simulations model. The arc-shaped gravity current is imposed in the eastern region (blue dash). The dashed rectangle marks the analysis domain (5×5 km^2) over Sendai Airport. MSL = mean sea level; AGL = above ground level; JST = Japan Standard Time; NICT = National Institute of Information and Communications Technology; ENRI = Electronic Navigation Research Institute.

An important aspect of the SBF is the three-dimensional (3-D) fine-scale structures that form and grow along the front. At its leading edge, the SBF is sometimes divided into a number of lobes and clefts, which are similar to the features of gravity current in laboratory tanks (Härtel et al., 2000; Mitsumoto et al., 1983; Simpson, 1969; Simpson & Britter, 1980; van der Wiel et al., 2017). At the shear zone between low-level onshore winds and ambient flows aloft, a train of Kelvin-Helmholtz billows (KHBs) may form and propagate seaward (Plant & Keith, 2007; Sha et al., 1991, 1993). These detailed structures (lobes/clefts, KHBs, winds, and vertical motions) of the SBF usually have a small scale of several hundred meters below the cloud base, which has been a difficulty in observational and numerical studies (Abbs & Physick, 1992; Geerts et al., 2006; Wood et al., 1999). Lidar that uses aerosols as a tracer can be utilized to measure the characteristics of SBF at high spatial and temporal resolutions (Mayor, 2011; Nakane & Sasano, 1986); dual-Doppler analysis techniques may further help to retrieve data regarding the winds and vertical motion (Atkins et al., 1995; Iwai et al., 2008; Newsom et al., 2008). However, there are few reports of dual-Doppler lidar that well captures the 3-D structures, winds, and temporal evolution of an SBF, as these detailed behaviors are esoteric in the limited area of lidar observation. Moreover, laboratory experiments usually treated gravity current as a continuous flow. It is unclear in realistic atmosphere how the short-term variations of gravity current in sea breeze regulate frontal structures.

Since the 1990s, a number of idealized numerical studies involving large eddy simulations (LES) have been conducted to investigate the fine-scale structures of sea breeze and their interactions with boundary layer disturbances (Cunningham, 2007; Fovel & Dailey, 2001; Jiang et al., 2017; Sha et al., 1991). In recent years, LES models have been coupled with a mesoscale model to simulate the boundary layer turbulence more realistically at given atmospheric conditions. In particular, the coupled mesoscale-to-LES models allow for an explicit resolution of both mesoscale weather and small-scale turbulence in the large domain of an entire city (F. Chen et al., 2011; G. Chen et al., 2015a; Mazzaro et al., 2017; Muñoz-Esparza et al., 2017). These numerical studies require a large amount of computational resources and have been prohibitive in past decades (Atkinson & Zhang, 1996; Martilli, 2007). With the even faster supercomputers in recent years, the mesoscale-to-LES modeling of the SBF may help us to revisit the earlier numerical studies and to provide further insight into the dynamics and impacts of sea breeze over complex surfaces (Crosman & Horel, 2010). Meanwhile, because of a lack of high-resolution observational data, the performance of mesoscale-to-LES models in simulating the 3-D fine-scale structures of SBF remains to be validated.

Here, we conduct dual-Doppler lidar measurement to reveal the detailed behavior of a typical SBF along the Pacific coast. We identify the fine-scale structures, local winds, and temporal variations of the SBF via 3-D visualization of the lidar analysis data. Using the nested mesoscale-to-LES models, we perform numerical experiments to further investigate the structures, dynamics, and evolution of the SBF as well as their impacts on local weather. We pay attention on the role of short-term disturbances of gravity current in regulating the variations of SBF structures. As the buildings may also induce eddies disturb SBF, we conduct another experiment without buildings as a comparison to depict how large changes occur in frontal structures, updrafts, and surface winds. The numerical results are compared with lidar observations to verify the forecasting ability of the state-of-the-art model system in coastal areas.

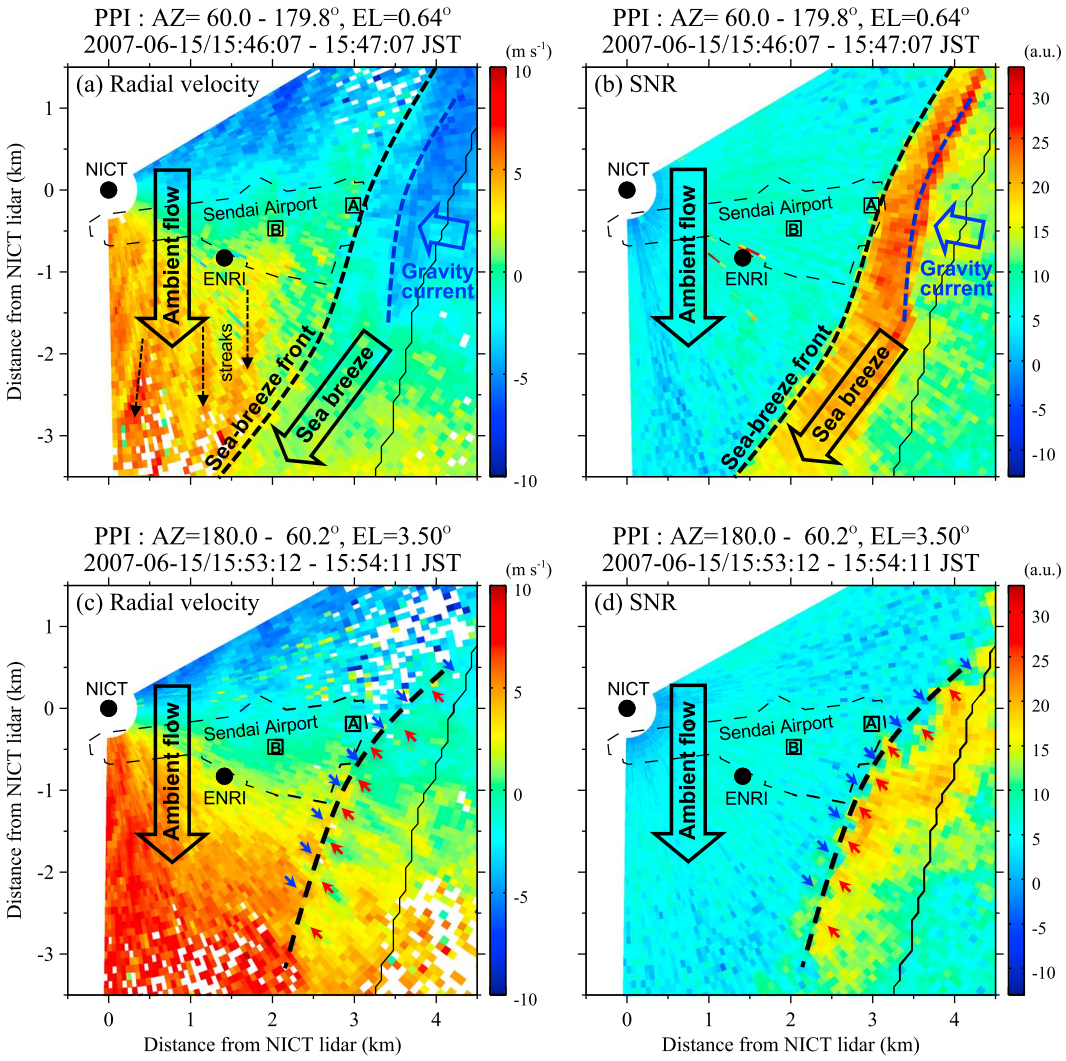

Figure 2. Observation networks and lidar PPI scans of the SBF over Sendai Airport. Radial velocity and SNR are derived from the scan of NICT lidar (a, b) near surface and (c, d) in the top of sea breeze. SBF and gravity current are denoted by the bold dashes in black and blue, respectively. The small arrows in (c) and (d) denote the elevated lobes/clefts with flows or SNR perturbations relative to the front. Circles denote the locations of the NCIT and ENRI lidars, and squares denote the two in situ meteorological sensors "A" and "B." PPI = plane position indicator; JST = Japan Standard Time; NICT = National Institute of Information and Communications Technology; ENRI = Electronic Navigation Research Institute; SNR = signal-to-noise ratio; SBF = sea-breeze front.

2. Data and Methods

2.1. Observation Data of the SBF Event

We focus on a well-defined SBF that occurred over Sendai Airport (38.135°N, 140.94°E) on the Pacific coast during the afternoon of 15 June 2007. On that day, the ambient flow was primarily characterized by an alongshore northerly wind, as a synoptic low system was located over the northwestern Pacific (Figure 1a). Throughout the afternoon, a SBF stayed at the east of Sendai Airport where the northeasterly wind from ocean converged with the northerly wind on land (Figure 1b). This feature of low pressure over ocean and alongshore ambient winds resembles a typical "backdoor" pattern, in which the inland intrusion of sea breeze is hampered and tends to form a sharp front near the coastline (Adams, 1997; Miller et al., 2003). As the SBF was nearly stagnant over airport for several hours, we are able to measure its fine-scale structures and associated temporal variations using local intensive observation network.

The observational data used in this study were obtained from a field investigation of sea breeze over Sendai Airport in June 2007 (Iwai et al., 2008). Dual-Doppler lidar observation was conducted using the National Institute of Information and Communications Technology (NICT) lidar and the Electronic Navigation

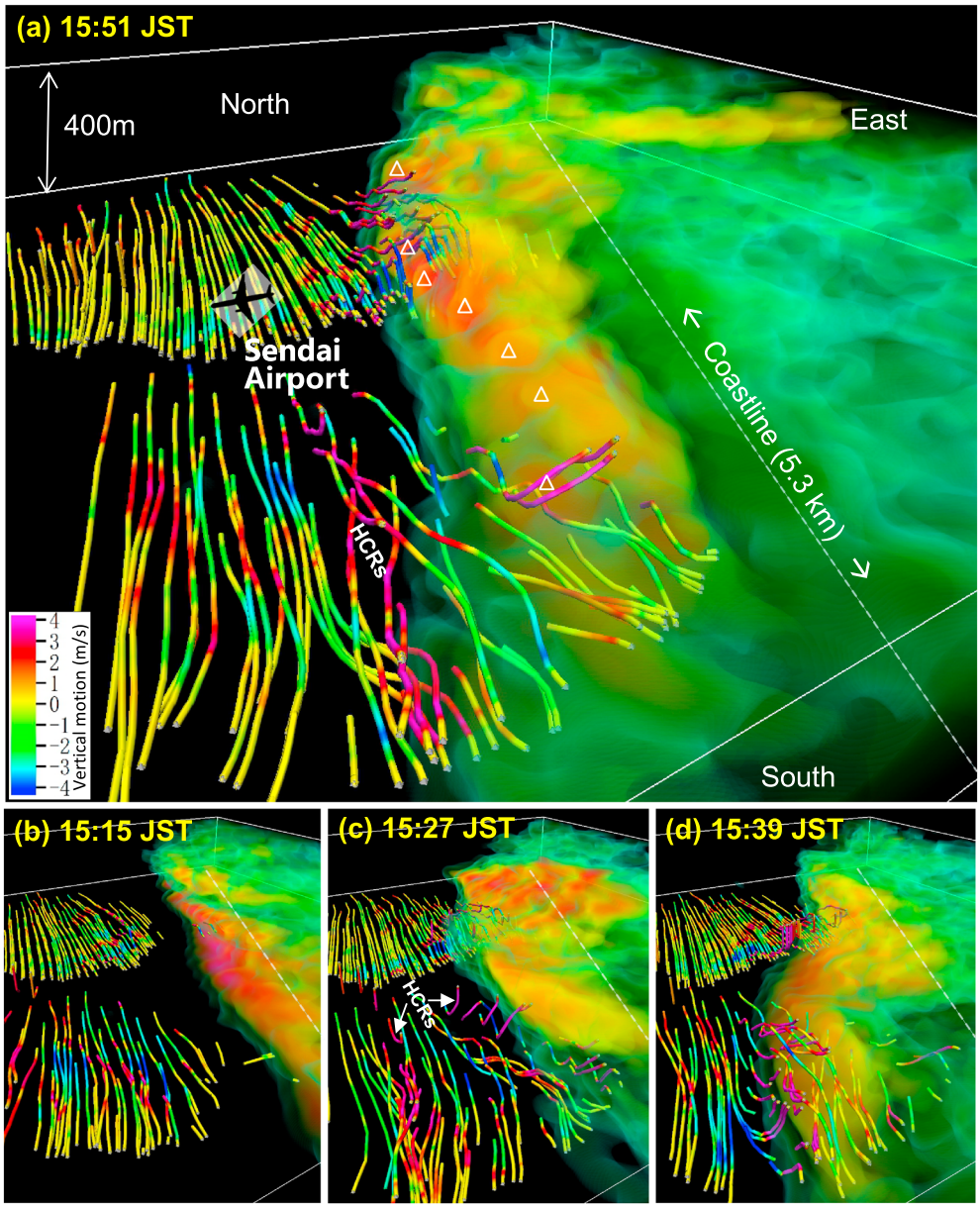

Figure 3. Three-dimensional structures of the observed sea-breeze front. Air flow (instantaneous streamline with red denoting rising motion) and aerosols (shaded for signal-to-noise ratio larger than 20 a.u.) retrieved from the volume scans of dual-Doppler lidar over the Sendai Airport domain at around (a) 15:51, (b) 15:15, (c) 15:27, and (d) 15:39 Japan Standard Time (JST). In (a) and (c), "HCRs" mark the streamwise updrafts associated with the horizontal convective rolls. The triangles in (a) mark the lobes.

Research Institute lidar. The two lidars were set up at the western edge and in the middle southern region of the airport, respectively (Figure 2). Four volume scans of the dual-Doppler lidar were completed from 15:10 to 15:56 Japan Standard Time (JST = UTC + 9) on 15 June, each having a duration of 10 min. One volume scan includes 10 sector plane position indicator (PPI) scans at elevation angles from ~0.5° to 5.0°. The radial velocities obtained from the dual-Doppler lidar were used to derive the horizontal winds and vertical motion. The specifications of two lidars and the method of wind derivation were detailed in Iwai et al. (2008). The signal-to-noise ratio from the NICT lidar, which had a better view of the coast in its PPI scans, was used to represent aerosol concentration. The retrieved wind and aerosol data were developed on a 3-D Cartesian grid at a 25-m resolution over a 5-km domain centered at Sendai Airport (see details in

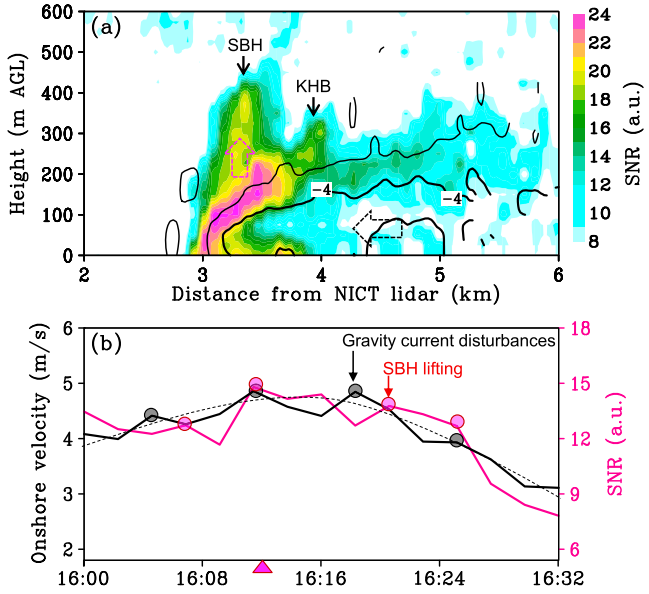

Figure 4. Vertical section and evolution of the observed sea-breeze front. (a) Radial velocity (contour, negative for onshore flow) and SNR (shaded, indicating aerosol concentration) derived from the range-height indicator scans of the NICT lidar at an azimuth angle of 95° (nearly normal to coast line) at 16:16 JST. (b) Temporal variations of onshore velocity below 200 m AGL at X = 3.5–5 km and frontal aerosols at 200–400 m AGL at X = 2.8–4 km. Dashed line denotes the running mean of onshore velocity. AGL = above ground level; SBH = sea-breeze head; KHB = Kelvin-Helmholtz billow; NICT = National Institute of Information and Communications Technology; SNR = signal-to-noise ratio.

Iwai et al., 2008). The 3-D data were visualized using the National Center for Atmospheric Research's Visualization and Analysis Platform for Ocean, Atmosphere, and Solar Researchers.

After the dual-Doppler lidar observation, the NICT lidar performed range-height indicator (RHI) scans with an azimuth angle of 95° (perpendicular to the coastline) from 16:00 to 16:32 JST. The RHI scans provided the spatial-temporal variations of inflows and aerosol structures of the SBF at a very high resolution of ~O (10) m and 1–2 min. On the other hand, the in situ meteorological sensors ("A" and "B" in Figure 2) at the eastern edge and middle locations of the airport were used to show the surface winds near the front and in the ambient air, respectively. The wind data at both sensors have a very high resolution of 3 s. Sensor B also provided temperature data at an interval of 6 s. From 15:10 to 16:30 JST, the active SBF was detected three times by the lidars and surface measurements, which is the focus of this study.

2.2. Mesoscale-to-LES Models and Configuration of Experiments

For a high-precision forecast of mesoscale weather at LES resolution, we designed an advanced nesting system in which a computational fluid dynamics (CFD) model is coupled to a mesoscale meteorological model with data assimilation (G. Chen et al., 2015a). The Japan Meteorological Agency-Nonhydrostatic Model (JMA-NHM) was employed to reproduce the mesoscale atmospheric conditions associated with the sea-breeze event (Saito et al., 2006). To improve forecast accuracy, a convective-scale data assimilation scheme using the local ensemble transform Kalman filter was implemented with the JMA-NHM at spatial resolutions up to 1.5 km (Miyoshi & Aranami, 2006; Seko et al., 2011). Hourly assimilated data were then used to make short-range forecasts downscaling to higher resolutions of 400 and 100 m. Both the ambient winds and SBF's position were well reproduced, though the frontal rising motion exhibited little local features in the mesoscale modeling (Figure 1b).

A building-resolving CFD model was employed to explicitly describe complex surfaces and large eddies in the inner domain (G. Chen et al., 2015a; Sha, 2002). The model solves the fully compressible Navier-Stokes equations using an algorithm of the semi-implicit method for pressure-linked equation revised code (Patankar, 1980). Dynamic impacts of surface geometries including the shape and height of buildings were handled by a block-off technique. The prescribed ground temperature from JMA-NHM at 100-m grids was used to set the building wall temperature, which was fixed during the short period of CFD modeling. Initial and lateral atmospheric conditions were provided by the JMA-NHM forecast at 15:50 JST, 15 June (Figure 1b). Both the lateral and upper boundary conditions were treated by an improved Orlanski-type radiation condition, so that they are free of reflection from gravity wave propagation (Orlanski, 1976). The model top was 1,200 m high, which was much higher than the sea-breeze depth (200–300 m) in this study. Another run with a lower model top of 700 m can produce similar results, and thus the current setting seems adequate. To capture the mesoscale evolution of the SBF, the CFD simulation was conducted over a 25 × 25-km^2 domain centered at Sendai Airport, with a uniform resolution of 10 m.

To represent the gravity currents from ocean (unresolved in mesoscale model) in CFD model, a perturbation of temperature (−1 K) and wind speed ($u' = -1$ and $v' = 1$ m/s) was imposed in the initial condition over sea surface (Figure 1b). Both the wind perturbation and the arc-shaped boundary of imposed gravity current were given comparable to the observed features via lidar (Figures 2a and 2b). The disturbance's location was displaced slightly east relative to the observation, giving a lag of 5–6 min in the CFD model for spin-up. The perturbations were added in the lowest layer below 200 m. The depth and wind perturbations of gravity current were also analogous to those observed by the lidar RHI scans that are shown later. The sensitivity of the model results to the above settings will be discussed in section 4.1. To simulate the life cycle of a gravity current disturbance, the CFD simulation was run

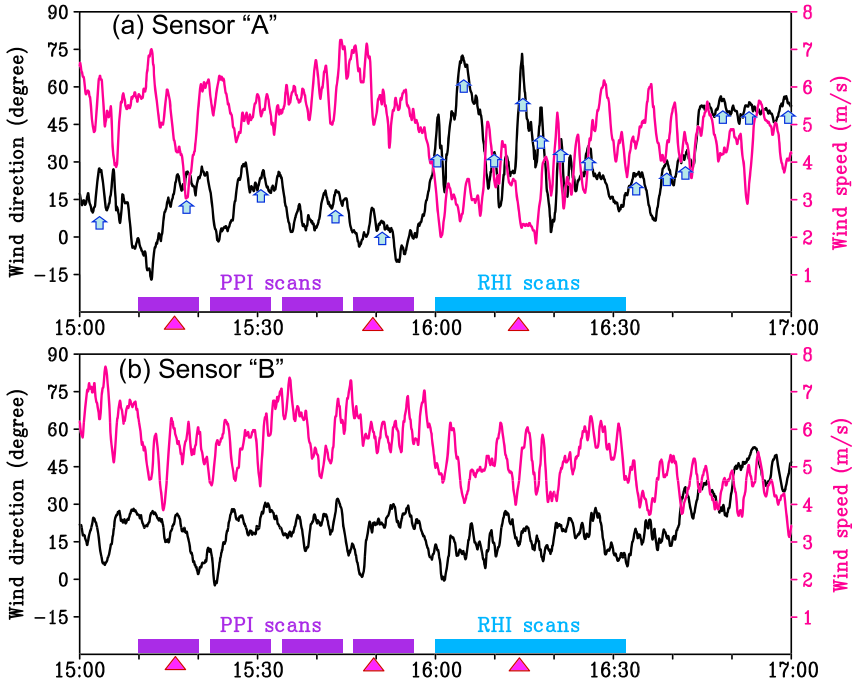

Figure 5. Surface winds observed at Sendai Airport during the sea breeze event. The locations of two sensors "A" and "B" are shown in Figure 2. Arrows in (a) denote the wind oscillations of increased direction and decayed speed, at an interval of ~12 (~5) min before (after) 16:00 JST. Triangles at *X* coordinate approximately denote the mature stages of the sea-breeze front, based on the visual criteria of frontal aerosols. The developing/decaying phases may be defined relative to the mature stages. The periods of the lidar observations are marked by the rectangles. PPI = plane position indicator; RHI = range-height indicator.

for 30 min with a time step of 1 s. Meanwhile, random cell perturbations were input into the initial field to achieve a fast growth of boundary layer turbulence (Jiang et al., 2017; Muñoz-Esparza et al., 2014). The cell perturbations continued to work at the lateral boundary and disturb the inflow during the simulation. Parallel computation of the CFD model was performed using the K Computer in Kobe, Japan. Recent studies suggested that coupled mesoscale-to-LES models can yield an improved simulation of convective rolls in the sea breeze over complex surfaces (G. Chen et al., 2015a, 2015b) or a realistic representation of boundary layer properties and turbulence structure through a diurnal cycle (Muñoz-Esparza et al., 2017).

3. Three-Dimensional Structures and Temporal Variations of the SBF Observed Over Sendai Airport

3.1. Fine-Scale Structures of the SBF Revealed by Lidar Analysis

First, we examine the horizontal patterns of wind and air mass associated with the SBF. Figures 2a and 2b show the near-surface conditions retrieved from the PPI scan at the lowest elevation angle. The airport domain is clearly divided by the SBF into two different flow regions: ambient northerly wind on land and northeasterly sea breeze near coastline (Figure 2a). On land, several streaks of surface winds with an along-flow orientation are embedded in the ambient flow. Such near-surface streaks indicates the activities of horizontal convective rolls (G. Chen et al., 2015a; Iwai et al., 2008). In the east half region of sea breeze, it features a relatively high signal-to-noise ratio, which corresponds to a large concentration of aerosol especially at a narrow zone behind the SBF (Figure 2b). An arc-shaped disturbance of onshore wind and aerosol (blue dash), indicating a gravity current in the sea breeze, tends to propagate onshore from the coast to the east of airport. The onshore velocity of the gravity current is 1–2 m/s higher than that of the preceding sea breeze. Figures 2c and 2d show another PPI scan for the upper part of the sea-breeze layer, which is at the height of 180–250 m at the coast (X = 3–4 km). Both radial velocity and aerosol exhibit regular concave-

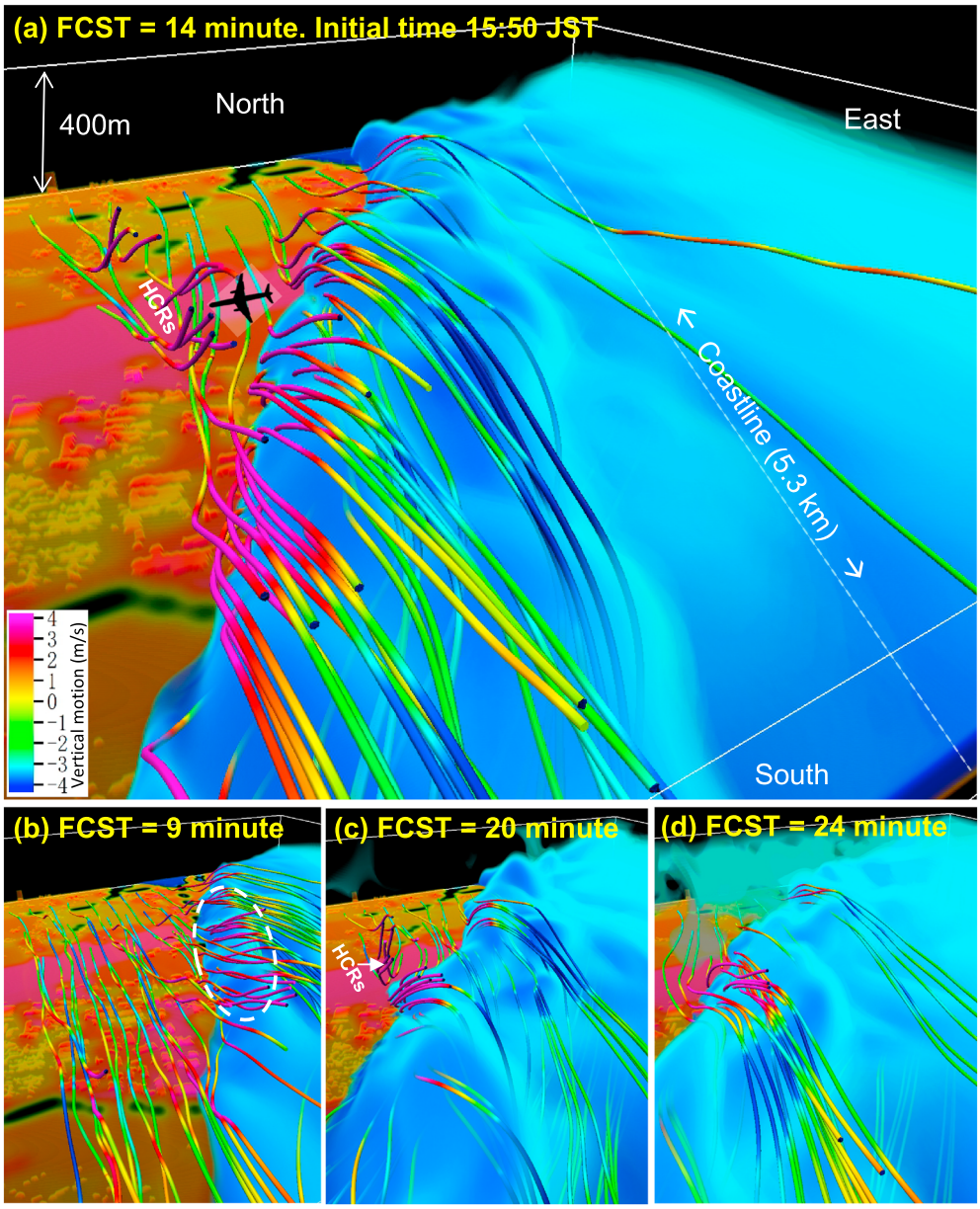

Figure 6. Three-dimensional structures of the simulated sea-breeze front. Air flow (instantaneous streamline, with red line denoting rising motion) and isothermal surfaces (shaded in blue for marine air mass with a temperature below 294 K and in red for land surface temperature above 295.5 K) simulated by the computational fluid dynamics experiment with buildings over Sendai Airport. Forecasts at (a) 14, (b) 9, (c) 20, and (d) 24 min. In (a) and (c), "HCRs" mark the streamwise updrafts associated with the horizontal convective rolls. In (b), the dashed ellipse marks the developing sea-breeze head due to gravity current.

convex perturbations at an interval of ~500 m. They suggest that the fine-scale structures of flow and air mass develop along the SBF.

We then investigate the 3-D structures of aerosol and winds retrieved from the volume scans of dual-Doppler lidar. Figure 3a shows a snapshot of the 3-D structures in the SBF's mature stage. The cool dense air features a high concentration of aerosols in the eastern half of the airport domain. At the leading edge, the SBF has a raised sea-breeze head (SBH) with a depth of ~300 m and an orientation from northeast to southwest. The SBH is evident adjacent to the airport runway, while it is less pronounced in the southern and northern areas. The raised SBH has a horizontal extent of ~3.5 km, which coincides with an arc-shaped disturbance

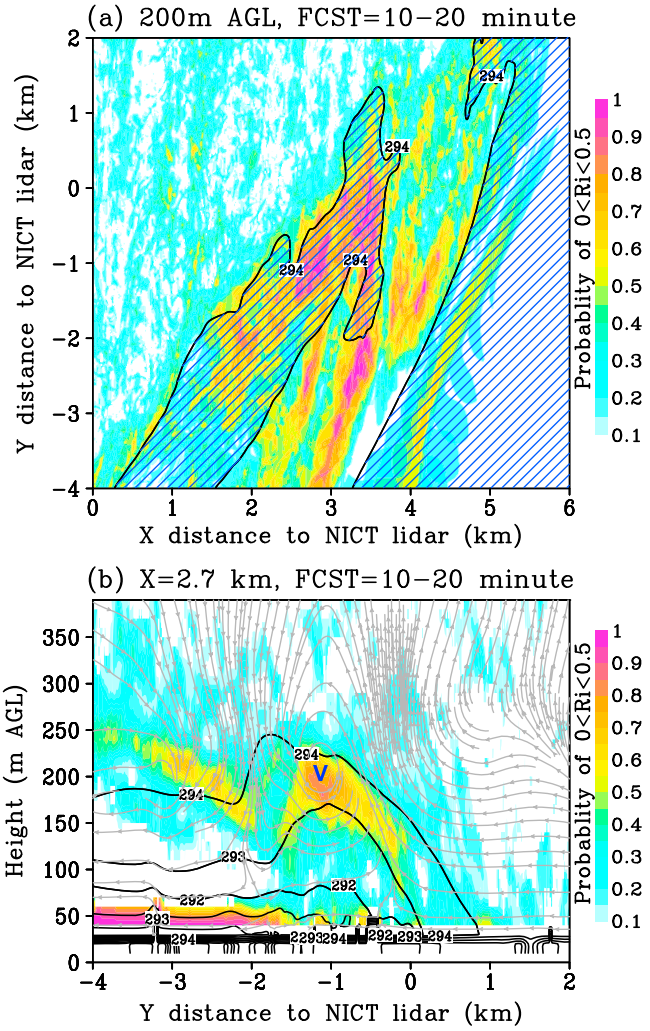

Figure 7. Instability condition at the sea-breeze head. (a) Horizontal distribution and (b) south-north vertical section of the probability (shaded) of small Richardson number ($0 < Ri < 0.5$) and the temperature below 294 K (contours). In (b), streamlines denote the flows relative to sea breeze. Character "V" marks the center of the vortex, which is collocated with the area of small *Ri*. AGL = above ground level; NICT = National Institute of Information and Communications Technology.

due to a sea-breeze gravity current (Figures 3a, 2a, and 2b). Along the foremost part of the SBH, a series of small-scale lobes, spaced ~500 m apart, are distinguishable (Figures 3a, 2c, and 2d). Strong updrafts occur along the frontal surface of the raised SBH in the northern area of the lidar analysis, while they are relatively weak in the southern area. In the warm area ahead of the southern part of the SBF, some streamwise bands of updrafts develop in the ambient northerly flow, which correspond to the near-surface streaks and horizontal convective rolls (Iwai et al., 2008). They are probably due to the thermal effect of the warm concrete surface (G. Chen et al., 2015b; Weckwerth et al., 1997) and may interact with SBF to enhance frontal updrafts (Fovel & Dailey, 2001).

Figures 3b–3d also show that the aerosols and flow patterns of the SBF vary markedly in the different volume scans of lidar. The raised SBH and lobes/clefts are pronounced at 15:15 JST, presenting an active SBF but at an eastern location relative to that at 15:51 JST (cf. Figures 3a and 3b). The SBH seems to break into two segments at 15:27 JST and propagates downstream at 15:39 JST, and the small-scale features of lobes/clefts become less distinguishable along the decaying SBF (Figures 3c and 3d). These different phases suggest that the frontal structures of the SBF may undergo evident short-term variations though the SBF itself has little inland propagation.

3.2. Temporal Variations of the SBF and Associated Surface Winds

The detailed temporal variations of the SBF can be further examined using the RHI scans from land to sea (Figure 4a). The aerosol concentration by SBH lifting may depict the 3-D structures of the SBF, while the onshore velocity behind the front denotes the strength of sea-breeze gravity currents (Iwai et al., 2011; Nakane & Sasano, 1986). Strong onshore inflow of −4 m/s is ~200 m deep, while the SBH attains a height of up to 400 m. Figure 4b shows that the onshore velocity strengthens during 16:00–16:16 JST and then decays gradually, with an amplitude of 1.5–2 m/s, which coincides well with the aerosol variations at the SBH. The mature phase of the SBF appears at 16:12–16:16 JST with maximum aerosols (Figure 4b), along with the other two peaks of the active SBF, which occur at 15:15 and 15:51 JST (Figures 3a and 3b), suggesting that the SBF has a short-term cycle of 25–35 min. Lidar observation also shows that the onshore winds exhibit oscillations at a very short period (~6 min) that are followed by aerosol disturbances, likely due to small-scale lobes/clefts. Such a close relationship between onshore velocity and SBH aerosols shows that the short-term cycles of gravity currents repeatedly reinforce the SBF (Figures 3 and 4b). The onshore propagation of gravity currents supports a subsequent presence of the fine-scale 3-D frontal structures, as shown in section 3.1 (Figure 3a). The observed features can be also used to optimize the simulation of gravity current in the CFD model as noted in section 2.2.

Surface winds may vary with the evolution of the SBF over Sendai Airport. At the east edge of the airport (sensor A), both wind direction and speed change markedly at around 16:00 (Figure 5a). It shifts from a northerly wind of ~6 m/s to a northeasterly wind of ~3 m/s, as the active SBF marches onshore and passes A (Figures 2a and 2b). Surface wind speed and direction exhibit higher-frequency oscillations at a period of ~5 min after 16:00 JST, compared to those of ~12 min before 16:00 JST (Figure 5a). It is closely related to the effect of the fine-scale structures of the SBF (Figure 4). Such oscillatory features of the SBF and surface winds were often noticed by the yachtsmen near the shore (Adams, 1997; Sun et al., 2002). At sensor B (~1 km to the west of sensor A), it is mainly affected in the land ambient wind during 15:00–16:40 JST (Figure 5b). Over there, both the temperature and wind direction is relatively stable (varying between 0° and 30°), and the mean wind speed decays slowly. Meanwhile, the frequency of wind perturbations undergoes minimal

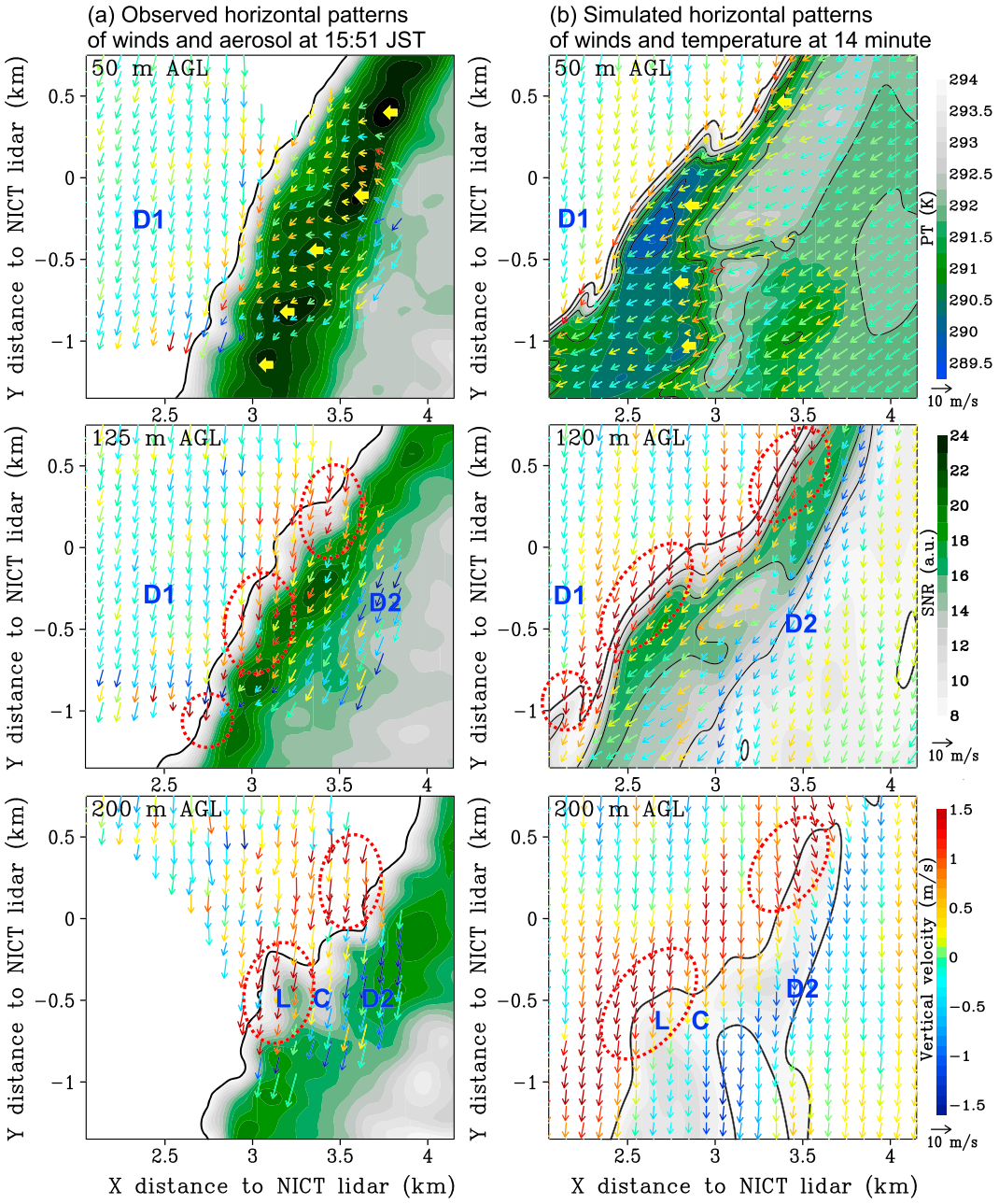

Figure 8. Enlarged views of the horizontal winds (vector), vertical velocity (color of vector), and air mass (shaded for aerosol or temperature) at the eastern edge of Sendai Airport derived from (a) dual-Doppler lidar analysis and (b) computational fluid dynamics model. Red circles denote the updrafts related to lobe "L" and cleft "C." "D1 and D2" denote downdraft zones. Bold arrows in yellow denote gravity current disturbances. AGL = above ground level; NICT = National Institute of Information and Communications Technology.

change throughout the period at sensor B. The differences in surface winds at two sensors suggest that the SBF may bring a strong contrast of local weather condition.

4. Fine-Scale Structures and Dynamics of the SBF Simulated by Mesoscale-to-LES Models

4.1. Three-Dimensional Structures of the Simulated SBF and Comparison With Lidar Observation

To further investigate the structures, dynamics, and impacts of an SBF, we perform numerical experiments as noted in section 2.2. Figure 6 shows the evolution of the simulated frontal structures and

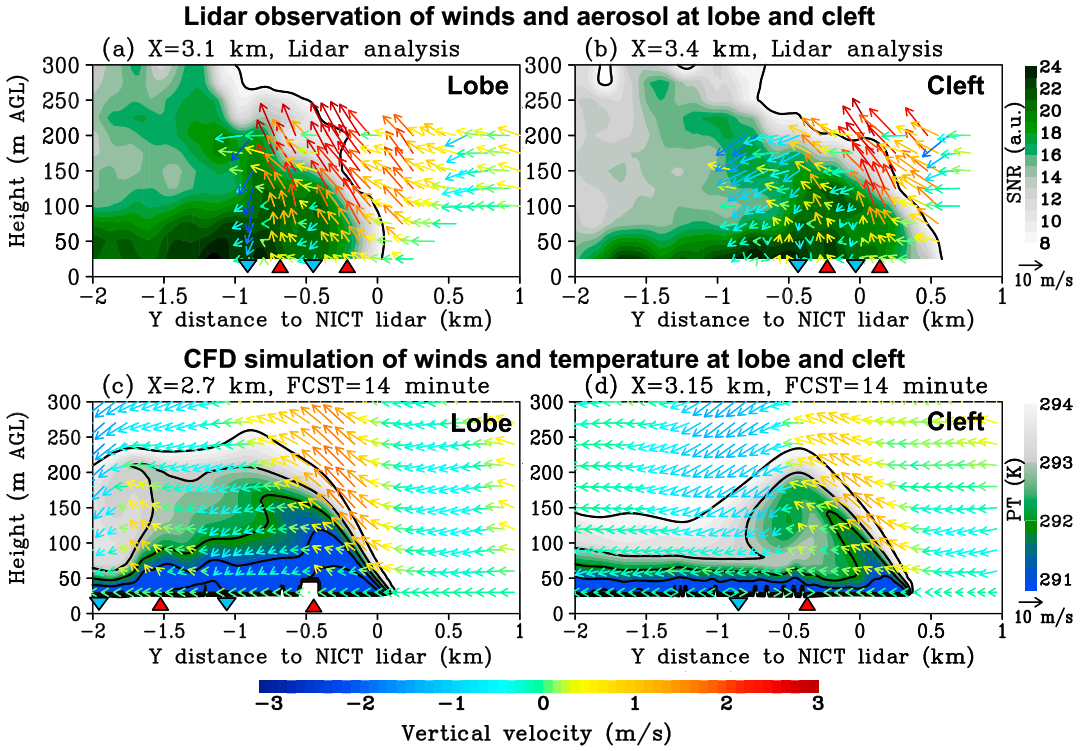

Figure 9. Fine-scale local winds and updrafts/downdrafts at lobe and cleft. Vertical cross sections of the winds (vector), vertical velocity (color of vector), and air mass (shaded for aerosol or temperature) are derived from (a, b) dual-Doppler lidar analysis and (c, d) computational fluid dynamics (CFD) model. Triangles denote the updraft-downdraft pairs associated with the Kelvin-Helmholtz billows. These sections are made at the lobe "L" and cleft "C," as shown in the bottom panels of Figure 8. AGL = above ground level; NICT = National Institute of Information and Communications Technology; SNR = signal-to-noise ratio.

flows over Sendai Airport. At the mature stage, the raised SBH of the marine cold air is double the depth (150–200 m) of the sea breeze (Figure 6a). The small-scale structures of lobes/clefts feature a series of cold air "noses" aligned regularly along the SBH. The instantaneous streamlines in Figure 6a show that continental air ascends at the wedge of the marine air and forms a strong rising motion at the frontal surface. Strong updrafts also occur in the cold dense air, particularly within lobes where the air parcel is forced upward. The lifted cold air parcels, however, tend to sink immediately behind the SBH as they are drifted downstream. This strong overturning of the sea breeze thus helps to trap air pollutants in the SBH. Compared to the dual-Doppler lidar analysis (cf. Figures 3a and 6a), numerical models satisfactorily capture the fine-scale structures of the active SBF and present more details related to the local winds. In the past, the activation of the SBF structures by gravity currents was usually studied in a laboratory or via idealized numerical experiments (Simpson, 1994, 1997). Most of numerical studies had been made at a horizontal grid spacing of ~100 m (Crosman & Horel, 2010, 2012; Robinson et al., 2013). To the best of our knowledge, this work represents the first success in modeling the observed 3-D structures of a mesoscale SBF at LES resolution with grid spacings on the order of several meters.

Numerical results also show that in its developing stage, the SBF becomes active at the coastline to the east of airport, where the SBH begins to be lifted and the small-scale lobes/clefts are growing (ellipse in Figure 6b). An analysis of surface temperature and pressure perturbations shows that the incoming gravity current begins to collide with the existing front at this stage (not shown). Then, the SBF moves inland and develops evident 3-D structures (Figure 6a). After the mature phase, the fully developed SBH breaks into two segments, as the two flanks of the arc-shaped gravity current continue to merge with the SBF (Figure 6c). A horizontal convective roll develops in the warm region (marked as "HCRs") and interacts with the SBF, which may lead to the local enhanced updrafts at the southern part of the airport (Fovel & Dailey, 2001). In the decaying stage, the raised SBH moves downstream toward the south due to an advection effect of the

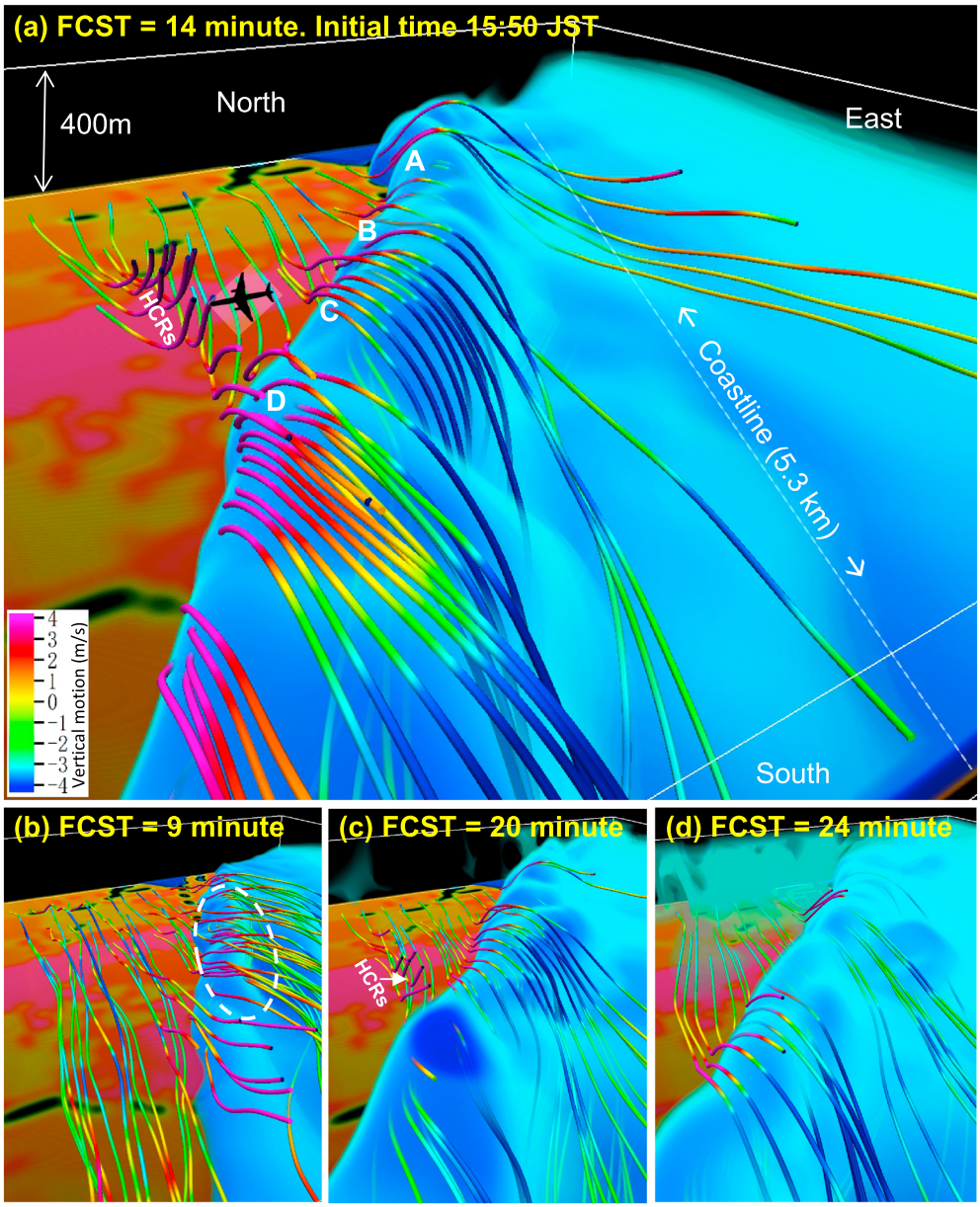

Figure 10. Same as Figure 6 but for the experiment without buildings. "A"–"D" mark the lobes in (a) corresponding to pressure perturbations in Figure 11b.

mean flow. Intense updrafts are still seen in the southern part of the SBF (Figure 6d). This life cycle of the simulated SBF is highly analogous to that observed by lidar (Figures 3a–3d). The satisfactory simulation is attributed to a reliable representation of both the background weather in the outer mesoscale model with data assimilation and the small-scale disturbances induced by buildings and short-term gravity currents in the inner CFD model.

In this study, the 3-D structures mostly appear at the leading edge of the SBF, while the disturbances behind the SBH are less evident. The features somewhat differ from the known pattern of the idealized SBF with offshore ambient winds, in which a train of KHBs develop behind the SBH (Miller et al., 2003; Sha et al., 1991, 1993; Simpson, 1994). The difference is likely due to the wind shear between continental air and sea breeze, which has an along-shore direction in this study. Correspondingly, instability condition with a small Richardson number mostly occurs along the foremost part of the SBH (Figure 7a). Over there, it favors the growth of small-scale disturbances such as KHBs (Plant & Keith, 2007; Sha et al., 1991, 1993). In the across-

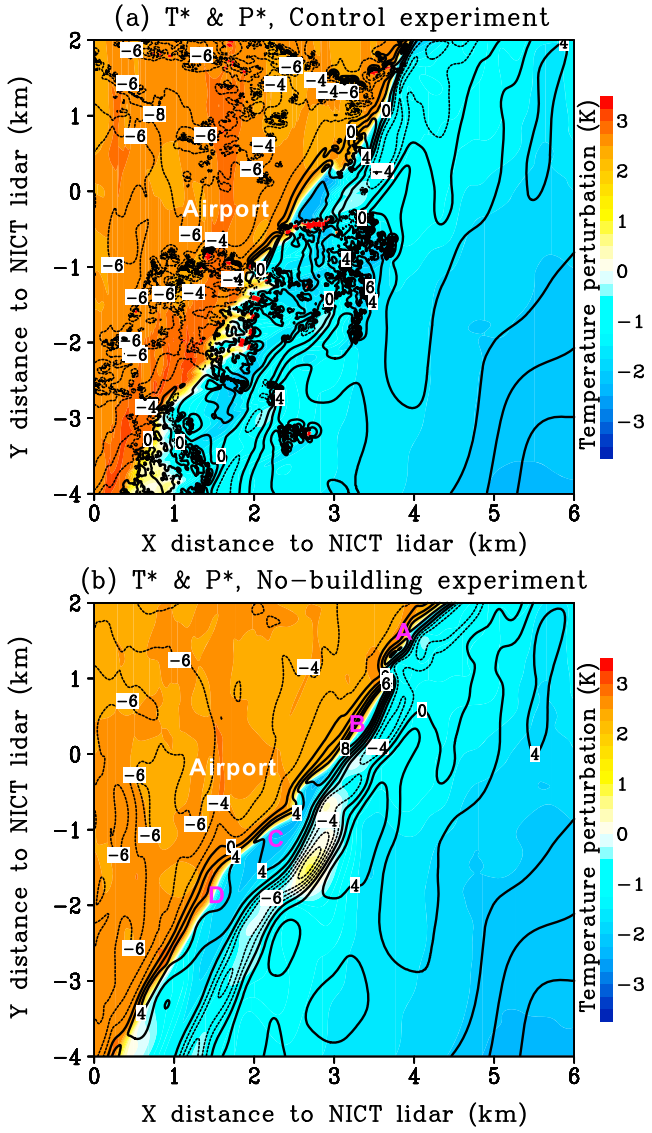

Figure 11. Near-surface temperature and pressure perturbations over airport simulated at 14 min. Perturbations are derived by removing the regional mean at 20 m above ground level in the computational fluid dynamics runs (a) with buildings and (b) without buildings. Shaded for temperature and contours for pressure at an interval of 2 Pa. "A"–"D" mark the local pressure perturbations associated with lobes in Figure 10a. NICT = National Institute of Information and Communications Technology.

shore direction, however, the offshore components of surface wind and low-level shear are relatively weak, which tends to induce shallow lifting (Liu & Moncrieff, 1996; Moncrieff & Liu, 1999). Another feature in this study is that the incoming density current head lasts for a short period and thus it reinforces the frontal structures temporarily. In the sensitive experiments with enhanced (reduced) amplitude of gravity current, the 3-D structures at the SBH become more (less) pronounced than those in Figure 6. Nevertheless, all experiments show that, as the gravity current decays after merging with SBF, the frontal structures begin to decline in the following minutes (figure not shown).

4.2. Formation of the Frontal Lobes and Localized Updrafts/Downdrafts

Using the high-resolution observational and modeling data, we further investigate the locally enhanced vertical motions at the SBF. Figure 8 shows an enlarged view of local winds and air mass at the northern domain of lidar analysis. Both the observation and simulation show that, near the surface, there is a frontal convergent zone between the northerly ambient flow and northeasterly sea breeze (upper panels of Figure 8). Another convergent zone appears ahead of the advancing gravity current, which leads to the ascending motions and locally raised cold air (bold arrows in yellow; Horner-Devine & Chickadel, 2017). As the two convergent zones merge, the small-scale features of the rising cold air develop into the frontal lobes at 100–200 m above ground level (middle and bottom panels of Figure 8). The temporary formation and growth of the lobes/clefts thus originate in the incoming short-term gravity currents and their pulsed collision at the SBF, while the movement of the SBF is quite slow. The scenario differs somewhat from that of a moving SBF with sustained density currents, in which the lobes/clefts can continue to form at the frontal head (Miller et al., 2003; Sha et al., 1991, 1993; Simpson, 1997). Enhanced frontal structures and ascending motions due to two colliding density currents are observed in a recent laboratory study (van der Wiel et al., 2017).

In addition to the forced upward motion in the sea breeze, ambient flow ascends at the wedge of the tilted SBF (Figure 9). The ascending motion intensifies significantly at the windward lobes, where the slope of the frontal surface is steeper than that at the clefts, resulting in localized strong updrafts at the SBF. Sinking motions are seen both in the prefrontal warm zone and in the rear zone of the SBH (Figures 8 and 9). The former is likely related to a compensation of the frontal updrafts (Miller et al., 2003; Nakane & Sasano, 1986; Sun et al., 2002). The latter is stronger and more extensive, as it is due to the sinking of lifted cold dense air downstream of the raised SBH and the isentropic flowing of warm air aloft (Figure 9b). Lidar analysis also shows some pairs of updrafts/downdrafts within the sea breeze (triangles in Figure 9a). These vortices are most evident downstream of the lobes and indicate the growth of the KHBs. The growth of these vortices is evident at the upper part of the SBH (i.e., 150–250 m above ground level), where the shear between sea breeze and ambient flow aloft leads to a small Richardson number ("V" in Figure 7b). The KHBs after their formation mainly drift southward along the front rather than seaward under ambient northerly winds. Numerical model reproduces some signatures of the KHBs but at a relatively long wavelength compared to that of lidar observations (cf. Figures 9a and 9b). As the aforementioned updrafts/downdrafts depend strongly on the fine-scale structures of the SBF, their general variations are regulated by the disturbances resulting from the gravity currents. These results underscore the need to observe and model the onshore-moving gravity currents at a scale of several kilometers to

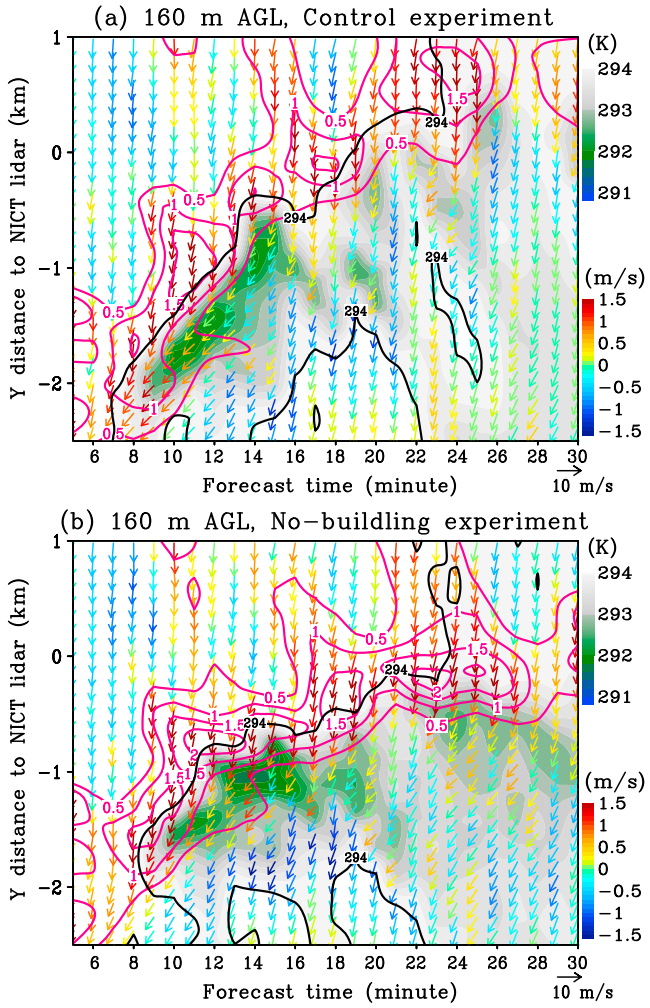

Figure 12. Temporal variations of the simulated frontal structures. The horizontal winds (vector), vertical velocity (color of the vector; red contours for updrafts), and air mass (shaded for temperature below 294 K) at the eastern edge of Sendai Airport are derived from the computational fluid dynamics runs (a) with buildings and (b) without buildings. AGL = above ground level; NICT = National Institute of Information and Communications Technology.

improve the short-term prediction of the SBF structures, turbulent features, and local vertical motions in coastal regions.

4.3. Impacts of Buildings on Frontal Structures and Local Winds

As the sea breeze is a shallow phenomenon, it can be subject to the influence of underlying surfaces. Because of the difficulty in resolving all buildings over a coastal city, it is currently not known how buildings regulate the fine-scale structures of a mesoscale SBF and associated local winds (Crosman & Horel, 2010). To address this key issue, we conduct a sensitive experiment with all buildings removed. The difference between two runs with and without buildings manifests an effect of buildings on SBF.

Figure 10 shows that the 3-D structures of simulated SBF in the simulation without buildings have a relatively high SBH, compared to those in Figure 6. The isothermal surface of the raised cold air is smoother, and thus, the small-scale perturbations are less evident. Correspondingly, the updrafts are stronger and more coherent along the SBF in the run without buildings (Figure 10). Further analysis shows that these fine-scale structures of the lobes at SBH (Figure 10a) are well collocated with the perturbations of surface pressure and low temperature (Figure 11b). As a comparison, in the run with buildings, the horizontal patterns of surface perturbations can be strongly disturbed and exhibit more localized features in built-up areas (Figure 11a). Pressure perturbation has a large magnitude up to 8 Pa in the run without buildings, while it is relatively small in that run with building obstacles. These results suggest that, in the presence of coastal sparse buildings, the building-induced small eddies can disturb the coherent features of mesoscale gravity currents, producing the local disturbances in frontal structures and winds. This situation differs somewhat from that of a densely built-up area, where the SBH is elevated due to surface drag (Jiang et al., 2017; Thompson et al., 2007).

To show the temporal variations of frontal structures and local winds, a south-north section is made at the eastern edge of the airport. Figures 12a and 12b show that the raised cold air is generally pronounced in the forecasts of 10–16 and 20–26 min, while its detailed variations differ markedly in the two runs after the forecast of ~8 min. The raised density current head also has a relatively low temperature in the run without buildings (Figure 12b). Frontal updrafts form near the developing lobes with a maximum magnitude of 1.5–2 m/s, which is stronger than that of 1–1.5 m/s in the run with buildings (cf. Figures 12a and 12b). Both the cold air and frontal updrafts exhibit regular oscillations with a very short period of 4–6 min, which is closely related to the lobes/clefts of the SBF. However, the detailed locations and timing of individual updraft maxima differ largely between the two runs.

We also expect the differences of surface winds in the two numerical experiments. Figures 13a and 13b show that, in the control run with buildings, the simulated surface winds shift from northerly to easterly after the forecast of 14 min, consistent with the observation at sensor A. Wind speed also decreases slightly and exhibits oscillatory features with a very period of 4–6 min. Figure 13c shows that, in the run without buildings, the sudden change in wind direction is decayed by ~5 min because the SBF is displaced south (Figures 10c, 10d, and 12b). These differences indicate that coastal buildings may regulate the variations of local winds by altering the frontal structures and positions. Compared to in situ measurements, the numerical experiment with buildings produces surface winds more similar to the observation than those produced without buildings (cf. Figures 13a–13c). This result highlights that a proper resolving of the mesoscale weather, boundary layer disturbances, and buildings in the coupled mesoscale-to-LES models may improve local weather prediction.

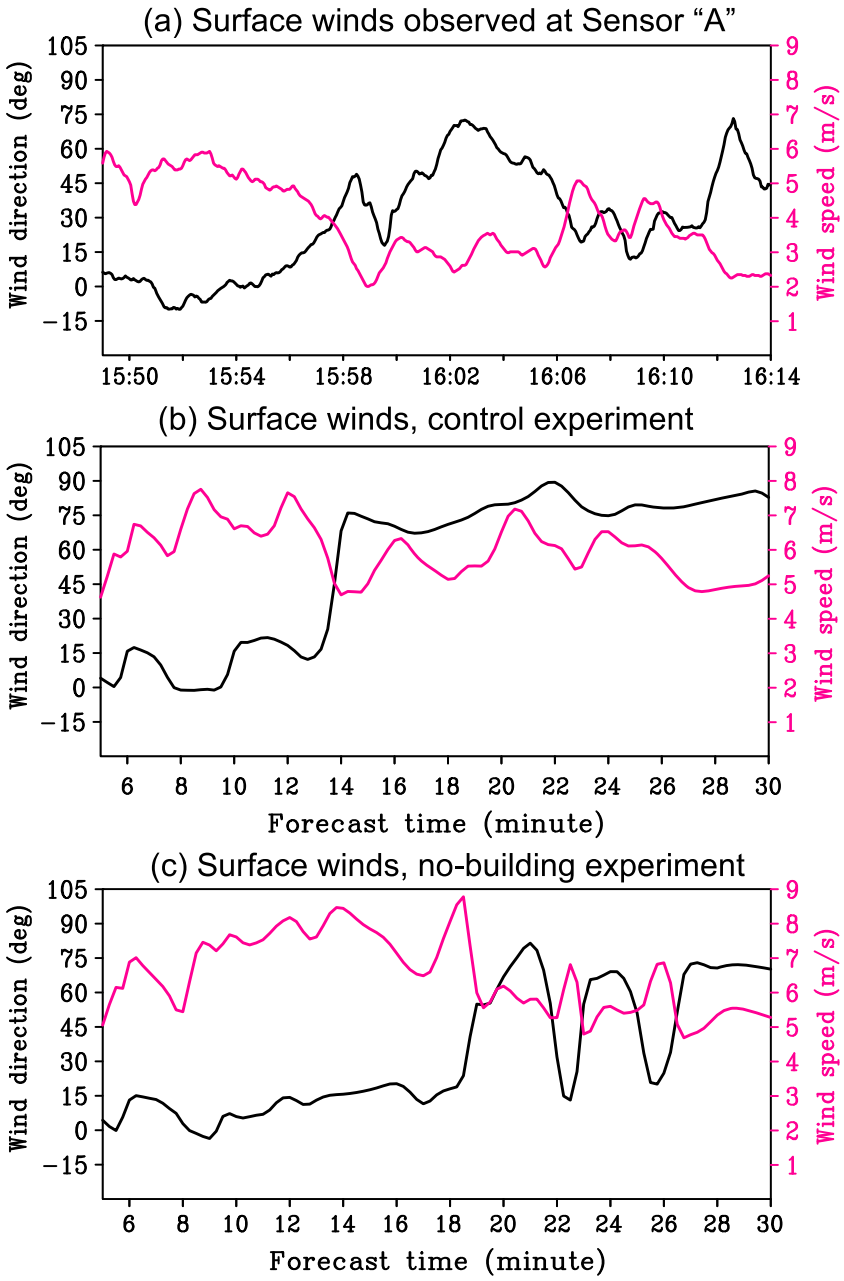

Figure 13. Temporal variations of surface winds at sensor "A". (a) Observation and in the computational fluid dynamics runs (b) with buildings and (c) without buildings. The location of sensor "A" is shown in Figure 2.

5. Summary and Discussion

In this study, we present an observation study of a sea-breeze event using dual-Doppler lidar and a numerical simulation using a LES model forced by a mesoscale prediction system that includes data assimilation features. We focus on how coupled mesoscale-to-LES methodology can be used to reproduce the structures of an SBF for the first time, which is validated through comparison to lidar observations, and provide insight into fine-scale structures and specific dynamics of the SBF.

Our analysis of dual-Doppler lidar observations shows that the backdoor-type SBF has evident 3-D structures with fine-scale lobes/clefts under alongshore ambient winds. The frontal structures and associated ascending/sinking motions are primarily driven by the disturbances of onshore-moving gravity currents

that collide with the nearly stagnant front line. The 3-D structures exhibit short-term oscillations due to the repeated arrivals of gravity current disturbances. The pattern differs somewhat from the well-known one of a moving SBF with sustained density currents under offshore ambient winds. As gravity currents feature mesoscale enhanced onshore velocities and aerosols, they are distinguishable in the lidar scans and indicate the predictability of 3-D frontal structures. Thus, short-range lidar can be applied to generate the early alerts of strong updrafts, wind shear, turbulence, and air pollutants associated with the SBF.

The coupled mesoscale-to-LES modeling further suggests that the incoming gravity currents can reinforce the SBH, produce small-scale lobes/clefts, and strengthen localized updrafts/downdrafts. Strong updrafts mostly occur near the windward lobes where marine cold air is forced upward and prefrontal warm air ascends at a relatively steep wedge of the tilted SBF's surface. These local disturbances mostly develop at the leading edge of an SBF, where the alongshore wind shear between continental flow and sea breeze is pronounced. Surface buildings are also found to disturb the coherent features of an SBF and regulate the detailed temporal variations of frontal structures and local winds. These simulated SBF structures, local winds, and their evolution are highly analogous to those of lidar and surface measurements. We suggest that an advent of mesoscale-to-LES models on supercomputers may improve the prediction of the SBF and facilitate understanding the associated dynamical processes and local impacts, particularly over coastal cities.

The coastal weather has a high variability due to the sea breeze, its interactions with mesoscale weather and boundary layer disturbances, and the effect of complex surfaces (e.g., Miller et al., 2003). It demands us to integrate the advanced observation and model systems for the coastal issues. One challenge is the remote sensing of the atmospheric disturbances propagating from oceanic surface, where in situ measurements are sparse (Soderholm et al., 2016; Wilbanks et al., 2015). To capture the gravity currents, lidar observations at a high resolution of ~O (100) m and a few minutes are required (Mayor, 2011). Another difficulty involves how the observed disturbances are assimilated into numerical models. Currently, most of the local meteorological models are not yet adequate for representing the rapidly changing small-scale disturbances (Sawada et al., 2015). Revolutionary numerical systems with a 100-m grid spacing that can complete data assimilation at a very fast cycle should be developed to make forecast possible (Miyoshi et al., 2016). Validation using observation data under various weather conditions will also help to improve the coupled mesoscale-to-LES models in the future. This study underscores the urgent need of these observational and numerical techniques for achieving a high-precision prediction of local weather and atmospheric environment near the coast.

Acknowledgments
This study was supported by the Strategic Programs for Innovative Research (SPIRE) funded by the Japan Ministry of Education, Culture, Sports, Science and Technology (MEXT) and the National Natural Science Foundation of China (Grant 41775094). The numerical calculations were performed using the K computer at RIKEN Advanced Institute for Computational Science (proposal numbers hp140220 and hp180194). We also thank two anonymous reviewers for their helpful comments to improve the article. The observational data were collected in a field experiment funded by the MEXT (Grant 19204046) through the collaboration of NICT, ENRI, JAXA, and Tohoku University. Observational data and LES-resolving forecasts used in this study are available at the website (https://pan.baidu.com/s/1tZAw4wi_EqYfIfN6LUocmA).

References

Abbs, D., & Physick, W. L. (1992). Sea-breeze observations and modeling: A review. *Australian Meteorological Magazine*, *41*, 7–19.

Adams, E. (1997). Four ways to win the sea breeze game, *Sailing World*, March, 44–49.

Atkins, N. T., Wakimoto, R. M., & Weckwerth, T. M. (1995). Observations of the sea-breeze front during CaPE. Part II: Dual-Doppler and aircraft analysis. *Monthly Weather Review*, *123*(4), 944–969. https://doi.org/10.1175/1520-0493(1995)123<0944:OOTSBF>2.0.CO;2

Atkinson, B. W., & Zhang, J. W. (1996). Mesoscale shallow convection in the atmosphere. *Reviews of Geophysics*, *34*(4), 403–431. https://doi.org/10.1029/96RG02623

Boyouk, N., Léon, J. F., Delbarre, H., Augustin, P., & Fourmentin, M. (2011). Impact of sea breeze on vertical structure of aerosol optical properties in Dunkerque, France. *Atmospheric Research*, *101*(4), 902–910. https://doi.org/10.1016/j.atmosres.2011.05.016

Chen, F., Kusaka, H., Bornstein, R., Ching, J., Grimmond, C. S. B., Grossman-Clarke, S., Loridan, T., et al. (2011). The integrated WRF/urban modelling system: Development, evaluation, and applications to urban environmental problems. *International Journal of Climatology*, *31*(2), 273–288. https://doi.org/10.1002/joc.2158

Chen, G., Zhu, X., Sha, W., Iwasaki, T., Seko, H., Saito, K., et al. (2015a). Toward improved forecasts of sea-breeze horizontal convective rolls at super high resolutions. Part I: Configuration and verification of a down-scaling simulation system (DS^3). *Monthly Weather Review*, *143*(5), 1849–1872. https://doi.org/10.1175/MWR-D-14-00212.1

Chen, G., Zhu, X., Sha, W., Iwasaki, T., Seko, H., Saito, K., et al. (2015b). Toward improved forecasts of sea-breeze horizontal convective rolls at super high resolutions. Part II: The impacts of land use and buildings. *Monthly Weather Review*, *143*, 1873–1894.

Crosman, E. T., & Horel, J. D. (2010). Sea and lake breezes: A review of numerical studies. *Boundary-Layer Meteorology*, *137*(1), 1–29. https://doi.org/10.1007/s10546-010-9517-9

Crosman, E. T., & Horel, J. D. (2012). Idealized large-eddy simulations of sea and lake breezes: Sensitivity to lake diameter, heat flux and stability. *Boundary-Layer Meteorology*, *144*(3), 309–328. https://doi.org/10.1007/s10546-012-9721-x

Cunningham, P. (2007). Idealized numerical simulations of the interactions between buoyant plumes and density currents. *Journal of the Atmospheric Sciences*, *64*(6), 2105–2115. https://doi.org/10.1175/JAS3947.1

Fovel, R. (2005). Convective initiation ahead of the sea-breeze front. *Monthly Weather Review*, *133*(1), 264–278. https://doi.org/10.1175/MWR-2852.1

Fovel, R., & Dailey, P. (2001). Numerical simulation of the interaction between the sea-breeze front and horizontal convective rolls. Part II: Alongshore ambient flow. *Monthly Weather Review*, *129*(8), 2057–2072. https://doi.org/10.1175/1520-0493(2001)129<2057:NSOTIB>2.0.CO;2

Geerts, B., Damiani, R., & Haimov, S. (2006). Finescale vertical structure of a cold front as revealed by an airborne Doppler radar. *Monthly Weather Review*, *134*(1), 251–271. https://doi.org/10.1175/MWR3056.1

Härtel, C., Carlsson, F., & Thunblom, M. (2000). Analysis and direct numerical simulation of the flow at a gravity-current head. Part 2. The lobe-and-cleft instability. *Journal of Fluid Mechanics*, *418*, 213–229. https://doi.org/10.1017/S0022112000001270

Horner-Devine, A. R., & Chickadel, C. C. (2017). Lobe-cleft instability in the buoyant gravity current generated by estuarine outflow. *Geophysical Research Letters*, *44*, 5001–5007. https://doi.org/10.1002/2017GL072997

Hu, X. M., & Xue, M. (2016). Influence of synoptic sea-breeze fronts on the urban heat island intensity in Dallas–Fort Worth, Texas. *Monthly Weather Review*, *144*(4), 1487–1507. https://doi.org/10.1175/MWR-D-15-0201.1

Inoue, T., & Kimura, F. (2004). Urban effects on low-level clouds around the Tokyo metropolitan area on clear summer days. *Geophysical Research Letters*, *31*, L05103. https://doi.org/10.1029/2003GL018908

Iwai, H., Ishii, S., Tsunematsu, N., Mizutani, K., Murayama, Y., Itabe, T., et al. (2008). Dual-Doppler lidar observation of horizontal convective rolls and near-surface streaks. *Geophysical Research Letters*, *35*, L14808. https://doi.org/10.1029/2008GL034571

Iwai, H., Murayama, Y., Ishii, S., Mizutani, K., Ohno, Y., & Hashiguchi, T. (2011). Strong updraft at a sea-breeze front and associated vertical transport of near-surface dense aerosol observed by Doppler lidar and ceilometer. *Boundary-Layer Meteorology*, *141*(1), 117–142. https://doi.org/10.1007/s10546-011-9635-z

Jiang, P., Wen, Z., Sha, W., & Chen, G. (2017). Interaction between turbulent flow and sea breeze front over urban-like coast in large-eddy simulation. *Journal of Geophysical Research: Atmospheres*, *122*, 5298–5315. https://doi.org/10.1002/2016JD026247

Liu, C., & Moncrieff, M. W. (1996). A numerical study of the effects of ambient flow and shear on density currents. *Monthly Weather Review*, *124*(10), 2282–2303. https://doi.org/10.1175/1520-0493(1996)124<2282:ANSOTE>2.0.CO;2

Martilli, A. (2007). Current research and future challenges in urban mesoscale modelling. *International Journal of Climatology*, *27*(14), 1909–1918. https://doi.org/10.1002/joc.1620

Mayor, S. D. (2011). Observations of seven atmospheric density current fronts in Dixon, California. *Monthly Weather Review*, *139*(5), 1338–1351. https://doi.org/10.1175/2010MWR3374.1

Mazzaro, L. J., Muñoz-Esparza, D., Lundquist, J. K., & Linn, R. R. (2017). Nested mesoscale-to-LES modeling of the atmospheric boundary layer in the presence of under-resolved convective structures. *Journal of Advances in Modeling Earth Systems*, *9*, 1795–1810. https://doi.org/10.1002/2017MS000912

Miller, S., Keim, B., Talbot, R., & Mao, H. (2003). Sea breeze: Structure, forecasting, and impacts. *Reviews of Geophysics*, *41*(3), 1011. https://doi.org/10.1029/2003RG000124

Mitsumoto, S., Ueda, H., & Ozoe, H. (1983). A laboratory experiment on the dynamics of the land and sea breezes. *Journal of the Atmospheric Sciences*, *40*(5), 1228–1240. https://doi.org/10.1175/1520-0469(1983)040<1228:ALEOTD>2.0.CO;2

Miyoshi, T., & Aranami, K. (2006). Applying a four-dimensional local ensemble transform Kalman filter (4D-LETKF) to the JMA Nonhydrostatic Model (NHM). *SOLA*, *2*, 128–131. https://doi.org/10.2151/sola.2006-033

Miyoshi, T., Kunii, M., Ruiz, J., Lien, G., Satoh, S., Ushio, T., et al. (2016). "Big data assimilation" revolutionizing severe weather prediction. *Bulletin of the American Meteorological Society*, *97*(8), 1347–1354. https://doi.org/10.1175/BAMS-D-15-00144.1

Moncrieff, M. W., & Liu, C. (1999). Convection initiation by density currents: Role of convergence, shear, and dynamical organization. *Monthly Weather Review*, *127*(10), 2455–2464. https://doi.org/10.1175/1520-0493(1999)127<2455:CIBDCR>2.0.CO;2

Muñoz-Esparza, D., Kosovi, B., Mirocha, J., & Beeck, J. V. (2014). Bridging the transition from mesoscale to microscale turbulence in numerical weather prediction models. *Boundary-Layer Meteorology*, *163*, 409–440.

Muñoz-Esparza, D., Lundquist, J. K., Sauer, J. A., Kosović, B., & Linn, R. R. (2017). Coupled mesoscale-LES modeling of a diurnal cycle during the CWEX-13 field campaign: From weather to boundary-layer eddies. *Journal of Advances in Modeling Earth Systems*, *9*, 1572–1594. https://doi.org/10.1002/2017MS000960

Nakane, H., & Sasano, Y. (1986). Structure of a sea-breeze front revealed by scanning lidar observation. *Journal of the Meteorological Society of Japan*, *64*(5), 787–792. https://doi.org/10.2151/jmsj1965.64.5_787

Newsom, R., Calhoun, R., Ligon, D., & Allwine, J. (2008). Linearly organized turbulence structures observed over a suburban area by dual-Doppler lidar. *Boundary-Layer Meteorology*, *127*(1), 111–130. https://doi.org/10.1007/s10546-007-9243-0

Orlanski, I. (1976). A simple boundary condition for unbounded hyperbolic flows. *Journal of Computational Physics*, *21*(3), 251–269. https://doi.org/10.1016/0021-9991(76)90023-1

Patankar, S. V. (1980). *Numerical heat transfer and fluid flow* (p. 214). New York: CRC Press/Taylor & Francis Group.

Plant, R. S., & Keith, G. J. (2007). Occurrence of Kelvin-Helmholtz billows in sea-breeze circulations. *Boundary-Layer Meteorology*, *122*(1), 1–15. https://doi.org/10.1007/s10546-006-9089-x

Robinson, F. J., Patterson, M. D., & Sherwood, S. C. (2013). A numerical modeling study of the propagation of idealized sea-breeze density currents. *Journal of the Atmospheric Sciences*, *70*(2), 653–668. https://doi.org/10.1175/JAS-D-12-0113.1

Saito, K., Fujita, T., Yamada, Y., Ishida, J. I., Kumagai, Y., Aranami, K., et al. (2006). The operational JMA nonhydrostatic mesoscale model. *Monthly Weather Review*, *134*(4), 1266–1298. https://doi.org/10.1175/MWR3120.1

Saito, K., Kunii, M., & Araki, K. (2018). Cloud resolving simulation of a local heavy rainfall event on 26 August 2011 observed in TOMACS. *Journal of the Meteorological Society of Japan*, *96A*(0), 175–199. https://doi.org/10.2151/jmsj.2018-027

Sawada, M., Sakai, T., Iwasaki, T., Seko, H., Saito, K., & Miyoshi, T. (2015). Assimilating high-resolution winds from a Doppler lidar using an ensemble Kalman filter with lateral boundary adjustment. *Tellus*, *67*(1), 23473. https://doi.org/10.3402/tellusa.v67.23473.

Seko, H., Miyoshi, T., Shoji, Y., & Saito, K. (2011). Data assimilation experiments of precipitable water vapor using the LETKF system: An intense rainfall event over Japan 28 July 2008. *Tellus*, *63A*, 402–412.

Sha, W. (2002). Design of the dynamics core for a new-generation numerical model of the local meteorology (in Japanese). *Kaiyo Monthly*, *2*, 107–112.

Sha, W., Kawamura, T., & Ueda, H. (1991). A numerical study on sea/land breezes as a gravity current: Kelvin–Helmholtz billows and inland penetration of the sea-breeze front. *Journal of the Atmospheric Sciences*, *48*(14), 1649–1665. https://doi.org/10.1175/1520-0469(1991)048<1649:ANSOSB>2.0.CO;2

Sha, W., Kawamura, T., & Ueda, H. (1993). A numerical study of nocturnal sea breezes: Prefrontal gravity waves in the compensating flow and inland penetration of the sea-breeze cutoff vortex. *Journal of the Atmospheric Sciences*, *50*(8), 1076–1088. https://doi.org/10.1175/1520-0469(1993)050<1076:ANSONS>2.0.CO;2

Simpson, J. E. (1969). A comparison between laboratory currents and atmospheric density currents. *Quarterly Journal of the Royal Meteorological Society*, *95*(406), 758–765. https://doi.org/10.1002/qj.49709540609

Simpson, J. E. (1994). *Sea breeze and local winds* (p. 234). Cambridge: Cambridge University Press.

Simpson, J. E. (1997). *Gravity currents in the environment and the laboratory* (p. 244). New York: Cambridge University Press.

Simpson, J. E., & Britter, R. E. (1980). A laboratory model of an atmospheric mesofront. *Quarterly Journal of the Royal Meteorological Society*, *106*(449), 485–500. https://doi.org/10.1002/qj.49710644907

Soderholm, J., McGowan, H., Richter, H., Walsh, K., Weckwerth, T., & Coleman, M. (2016). The Coastal Convective Interactions Experiment (CCIE): Understanding the role of sea breezes for hailstorm hotspots in eastern Australia. *Bulletin of the American Meteorological Society*, *97*(9), 1687–1698. https://doi.org/10.1175/BAMS-D-14-00212.1

Sun, J., Burns, S. P., Lenschow, D. H., Banta, R., Newsom, R., Coulter, R., et al. (2002). Intermittent turbulence associated with a density current passage in the stable boundary layer. *Boundary-Layer Meteorology*, *105*(2), 199–219. https://doi.org/10.1023/A:1019969131774

Thompson, W. T., Holt, T., & Pullen, J. (2007). Investigation of a sea breeze front in an urban environment. *Quarterly Journal of the Royal Meteorological Society*, *133*(624), 579–594. https://doi.org/10.1002/qj.52

van der Wiel, K., Gille, S. T., Smith, S. G. L., Linden, P. F., & Cenedese, C. (2017). Characteristics of colliding sea breeze gravity current fronts: A laboratory study. *Quarterly Journal of the Royal Meteorological Society*, *143*(704), 1434–1441. https://doi.org/10.1002/qj.3015

Weckwerth, T. M., Wilson, J. W., Wakimoto, R. M., & Crook, N. A. (1997). Horizontal convective rolls: Determining the environmental conditions supporting their existence and characteristics. *Monthly Weather Review*, *125*(4), 505–526. https://doi.org/10.1175/1520-0493(1997)125<0505:HCRDTE>2.0.CO;2

Wilbanks, M. C., Yuter, S. E., De Szoeke, S. P., Brewer, W. A., Miller, M. A., Hall, A. M., & Burleyson, C. D. (2015). Near-surface density currents observed in the Southeast Pacific stratocumulus-topped marine boundary layer. *Monthly Weather Review*, *143*(9), 3532–3555. https://doi.org/10.1175/MWR-D-14-00359.1

Wood, R., Stromberg, I. M., & Jonas, P. R. (1999). Aircraft observations of sea-breeze frontal structure. *Quarterly Journal of the Royal Meteorological Society*, *125*(558), 1959–1995. https://doi.org/10.1002/qj.49712555804